# Resolving a merger in a hyper-luminous submillimeter galaxy at z=2.82

R. W. Perry<sup>1\*</sup>, S. C. Chapman, <sup>1,2,3</sup> Ian Smail, <sup>4</sup> F. Bertoldi<sup>5</sup>

- <sup>1</sup>Department of Physics and Atmospheric Science, Dalhousie University, Halifax, NS, B3H 4R2, Canada
- <sup>2</sup>NRC Herzberg Astronomy and Astrophysics, 5071 W Saanich Rd, Victoria, BC V9E2E7, Canada
- <sup>3</sup>Department of Physics and Astronomy, University of British Columbia, 6224 Agricultural Rd, Vancouver, BC V6T1Z1, Canada
- <sup>4</sup> Centre for Extragalactic Astronomy, Department of Physics, Durham University, South Road, Durham DH1 3LE

Accepted XXX. Received YYY; in original form ZZZ

#### ABSTRACT

We present the resolved properties of the z=2.82 Hyper Luminous Infrared Galaxy (HyLIRG) HS1700.850.1, the brightest 850 $\mu$ m source found in the SCUBA-2 followup to the Keck Baryonic Structure Survey fields (S<sub>850 $\mu$ m</sub> =19.5 mJy), and amongst the most luminous starbursts known at any redshift. Using the IRAM-NOEMA interferometer in the highest resolution Aconfiguration, we resolve the source into two components separated by ~8 kpc, visible as blue shifted and red shifted  $^{12}$ CO(5-4) lines, exhibiting the expected kinematic properties of a major merger between two gas-rich galaxies. The combined merger system is traced over 2.3" or 18.4 kpc. Each component of the merger shows ordered gas motions suggestive of a massive, turbulent disk. We measure the dynamical masses of the blue and red disks as  $(1.5 \pm 0.2) \times 10^{11}$  M $_{\odot}$  and  $(0.71 \pm 0.22) \times 10^{11}$  M $_{\odot}$  respectively. The more massive disk component shows broad wings in the CO line, offset by ~3 kpc from the disk centroid along the major axis, and extending to velocities ~  $\pm 1000$  km s $^{-1}$  from systemic velocity. We interpret this as either a possible bipolar outflowing component, or more likely a warping or tidal structure in the CO disk. Comparing the properties of HS1700.850.1 to other submillimeter detected galaxies with comparably bright 850 $\mu$ m luminosities suggests that ongoing gas-rich mergers, or at least a clustered/group environment lead to these most extreme starburst phases.

Key words: galaxies: kinematics and dynamics – submillimeter: galaxies – galaxies: high-redshift

# 1 INTRODUCTION

Our knowledge of the history of star formation in the Universe has grown dramatically with the discovery of sub-millimeter galaxies (SMGs - Smail et al. 1997; Barger et al. 1998; Hughes et al. 1998; Hodge & da Cunha 2020). The population was first detected using the Submillimetre Common User Bolometer Array (SCUBA) on the James Clerk Maxwell Telescope (JCMT), and many studies since have dissected the SMG population to further understand their role in the evolution of galaxies in the Universe (Chapman et al. 2005; González et al. 2011). SMGs are a massive, gas-rich population which have extremely high luminosities ( $L_{IR} \sim 10^{12} - 10^{13} L_{\odot}$ ), and are typically understood to be dust obscured galaxies that are undergoing a high star-formation rate episode (SFR  $\sim 10^2 - 10^3 \, \mathrm{M}_{\odot}$ yr<sup>-1</sup>; Swinbank et al. 2014; Michałowski et al. 2017). The brighter SMGs ( $S_{850\mu m} \sim 5 - 10 \text{ mJy}$ ) are a relatively rare phenomenon, with space densities of  $10^{-5}$  to  $10^{-6}$  Mpc<sup>-3</sup> (Dudzevičiūtė et al. 2020). Their rarity may be partly because on average, these galaxies have short depletion timescales (≃200 Myr; e.g., Birkin et al. 2021), due to their enhanced SFRs. The highest volume density of SMGs occurs at  $z \sim 2-3$ , indicating that they are coeval with the peak epoch of star formation (Chapman et al. 2003a, 2005; Simpson et al. 2014). With the advent of ALMA analysis of an unbiased sample, and the detailed multi-wave followup of the ALMA-identified counterparts, SMGs are now established as likely progenitors of the present day massive elliptical galaxies (e.g., Dudzevičiūtė et al. 2020).

At the extreme bright end, SMGs as luminous as  $S_{850\mu m} \sim 20 \text{ mJy}$ have been identified in wide-field surveys (e.g., Pope et al. 2006; Geach et al. 2017; Lacaille et al. 2019; Simpson et al. 2020). The implied high dust masses ( $\sim 1.1 \times 10^9 M_{\odot}$ ; e.g., Birkin et al. 2021) and SFRs (>  $1000 \,\mathrm{M_{\odot} \, yr^{-1}}$ ) together with compact sizes (~  $2.4 \pm 0.2 \,\mathrm{kpc}$ ; e.g., Simpson et al. 2015; Gullberg et al. 2019) suggest they must be maximally forming stars (e.g., Younger et al. 2008). A key question is therefore what causes these SMGs to be so luminous? There is now direct evidence that some SMGs are likely starburst-dominated major mergers, through multiple CO gas components and/or disturbed kinematics (e.g., Chapman et al. 2003b; Tacconi et al. 2006; Bothwell et al. 2010; Engel et al. 2010; Ivison et al. 2011, 2013; Riechers et al. 2011). This has been supported by simulations (e.g., Swinbank et al. 2008; Narayanan et al. 2010; Hayward et al. 2011, 2012; McAlpine et al. 2019). However, other mechanisms that drive extreme SFRs may also power SMGs, such as cold mode accretion (CMA; e.g., Kereš et al. 2005; Dekel et al. 2009a,b). In CMA-driven galaxies, star formation is sustained by smooth infall and accretion of gas-rich material, and as a consequence are constantly forming stars at high rates. The CMA streams that feed star formation can cause the disk to break up into giant clumps if they have a high enough gas fraction and degree of turbulence. The clumps then potentially migrate

<sup>&</sup>lt;sup>5</sup> Argelander-Institute of Astronomy, Bonn University, Auf dem Hugel 71, D-53121 Bonn, Germany

ryan-perry@dal.ca

inward and merge into a spheroid (Dekel et al. 2009a,b). Dekel et al. (2009a) advocated that the CMA phenomenon could power SMGs, and the work has been extended by others (Fardal et al. 2001; Finlator et al. 2006; Davé et al. 2010; Narayanan et al. 2015) whereby SMGs are massive galaxies sitting at the centers of deep potential wells and fed by smooth accretion. Carilli et al. (2010) and Hodge et al. (2012) have provided evidence that one of the most luminous SMGs known in the Universe (GN20) may be driven in this manner, although it also resides in a dense protocluster and may have very recently experienced a major merger.

Observations of the morphology and kinematics of molecular gas in SMGs is likely the most direct route to understanding the physical mechanisms behind their intense star formation. Shapiro et al. (2008) derived a framework for interpreting the growing body of resolved kinematics in distant galaxies, advocating ways to distinguish between a gas-rich merger model and a CMA model through observations of the gas dynamics and distribution. A merger would be represented by tidally disturbed gas with a starburst nucleus, while a well-defined disk with a smooth rotation curve would be indicative of CMA. The large-scale gravitational torques induced by gas-rich major mergers are efficient at removing and redistributing angular momentum (Barnes & Hernquist 1996), thereby funnelling the cold molecular gas into the galaxy's center and producing a nuclear starburst. Local ULIRGs (e.g., Downes & Solomon 1998; Bryant & Scoville 1999) and even high resolution simulations of SMGs resulting from mergers (e.g., Narayanan et al. 2009) show gas reservoirs concentrated in the central kpc or two. Less extreme, but still massive star forming galaxies at z > 2 have shown significant evidence for kinematics of large disk galaxies, with star formation sometimes occurring in ring-like structures at large radii (e.g., Genzel et al. 2008; Förster Schreiber et al. 2009), with disks broken into multiple giant clumps of ~1 kpc and 10<sup>9</sup> M<sub>☉</sub> (Förster Schreiber et al. 2006; Genzel et al. 2008). Tacconi et al. (2010) even found evidence for clumpy CO emission extending over these disks. Elmegreen & Elmegreen (2006) and Elmegreen et al. (2009) emphasized that CMA could naturally generate large, clumpy disk galaxies.

HS1700.850.1, one of the brightest SMGs in the Universe (Chapman et al. 2015b) with  $S_{870\mu\text{m}}$ = 19.5±1.9 mJy as measured by the Submillimeter Array (SMA), was discovered in the Keck Baryonic Structure Survey (KBSS) fields (e.g., Rudie et al. 2012.) The HS1700+64 field was imaged by SCUBA-2 with the JCMT to the  $850\mu m$  confusion limit as part of the submm-wave followup of 15 KBSS fields, covering  $\sim 0.2 \text{ deg}^2$  (Lacaille et al. 2019; Hill et al. 2019). The HS1700+64 field contains a massive proto-cluster at z =2.30 (Steidel et al. 2005), and given the proximity of HS1700.850.1 to the cluster centre ( $\sim 1'$  separation), it was initially thought to be a cluster member (Chapman et al. 2015a). A followup mm-wave spectral survey revealed the redshift to be z = 2.816, well behind the protocluster, and in fact inhabiting a relative void in the Lymanbreak galaxy (LBG) redshift distribution of this field (Chapman et al. 2015b). <sup>12</sup>CO gas properties of HS1700.850.1 exhibit a strong double peaked line profile (Chapman et al. 2015b), but the authors could not determine whether it was more consistent with a rotating disk or a merging system due to the low spatial resolution of the spectral imaging (beam size  $\sim 3.5'' \times 2.7''$ ). One piece of evidence in favour of a merger was the R<sub>53</sub> CO line ratio differences between the two line peaks, which would otherwise imply an inhomogeneous interstellar medium (ISM) within the system if it were a single large disk rather than two merging components, although we note that the uncertainties on the ratios make this an inconclusive result. In this paper, we study HS1700.850.1 at high spatial resolution using the IRAM-NOEMA interferometer, resolving the double-peaked CO line of the bright source into two components suggestive of a merger. This paper has the goal of determining whether the prodigious SFR of the source is consistent with a major merger explanation, characterizing the source in detail (§ 3), and exploring the implications (§ 4). In § 5 we present our summary and conclusions.

We use cosmological parameters  $\Omega_m = 0.286$ ,  $\Lambda_0 = 0.714$ , and  $H_0 = 69.6$  km s<sup>-1</sup> Mpc<sup>-1</sup> throughout the paper; at z = 2.816, this corresponds to an angular scale of 7.995 kpc arcsec<sup>-1</sup>.

#### **2 OBSERVATIONS**

The following sections outline the detailed observations and methods used to gather the data analyzed throughout the rest of the paper.

# 2.1 IRAM-NOEMA

We observed the redshifted CO(5-4) emission line (rest-frame = 576.3 GHz) in A-configuration in HS1700.850.1 using the IRAM-NOEMA tuned to 150.7 GHz. Observations were taken on March 9 and 10, 2015, using the six-antenna sub-array with an exposure time of 14,120 sec and a pointing center: 17:01:17.779, +64:14:37.85, J2000.0. Flux calibration was achieved by observing various calibrators (3C273, 3C345, B0234+285, B1749+096), while the quasar B1300+580 was used as a phase and amplitude calibrator. Data was processed using the most recent version of the GILDAS software. We resampled the cubes in 90 km s<sup>-1</sup> channels, and imaged them using the GILDAS suite mapping. A beam size of  $0.78'' \times 0.41''$ along a position angle 59 degrees East of North was achieved from the combined tracks. To obtain flux measurements, we deconvolved the visibilities using the CLEAN task. We combined the visibilities with natural weighting and inverted the data to an image with 0.13" pixels, calibrated in units of Jy beam<sup>-1</sup>. We analyzed data from both the WIDEX and ASIC correlators, finding integrated line plus continuum detections of  $19.7\sigma$  and  $20.6\sigma$  respectively. HS1700.850.1 is clearly spatially resolved well beyond the beam, showing a Full Width Half Maximum (FWHM) extent of  $1.3'' \times 0.7''$  with a major axis PA of 48 degrees East of North. The integrated one-dimensional spectrum of the total system and the red and blue intensity maps are shown in Figure 1, and the moment maps are shown in Figure 2 (see §3.1.) The 151 GHz continuum sensitivity (in the collapsed 3.8 GHz band) is 0.061 mJy ( $1\sigma$ ), detecting the source with a 10.1 $\sigma$  peak flux. The combined NOEMA 151 GHZ A+D config map reaches slightly deeper at 0.05 mJy ( $1\sigma$ ). HS1700.850.1 is the only source detected signficantly (>  $5\sigma$ ) in the map.

# 2.2 SMA

Followup SMA observations were performed over four different tracks: September 26 and 28, 2014 in the extended configuration (achieving a beam size  $\sim 0.72'' \times 0.74''$  in the combined tracks), and October 21 and 29, 2014 in the compact configuration (beam size  $\sim 2.5'' \times 1.9''$ ). A subset of these observations were previously described in Chapman et al. (2015b). Here we combine additional data obtained, and separately analyze the compact and extended configuration data. All tracks were taken in good weather ( $\tau_{225\text{GHz}} < 0.07$ ) with a total on-source integration time of approximately 6 hr (Compact) and 11 hr (Extended). The upper sideband (USB) was tuned to 345 GHz, and combined with the lower sideband (LSB) for an effective bandwidth of  $\sim 4$  GHz at 340 GHz, which yielded a final RMS in the combined observations of 0.9 mJy. The combined map still detects only one significant  $> 5\sigma$  source (HS1700.850.1). The

pointing centre was the same as that for the NOEMA observations described above. The data was calibrated using the MIR software package (Scoville et al. 1993), modified for the SMA. Passband calibration was done using 3C 84, 3C 111, and Callisto. The absolute flux scale was set using observations of Callisto and is estimated to be accurate to better than 20%. Time-dependent complex gain calibration was done using 1858+655 (0.6 Jy, 21.8° away) and 1827+390 (1.8 Jy, 37.7° away). In the compact track we detect the source at  $9.3\sigma$ ,  $S_{890\mu m}$  = 19.5 ± 1.9 mJy, after CLEANing the image down to  $1\sigma$ . The centroid lies at  $\alpha(J2000) = 17:01:17.767$  and  $\delta(J2000) =$ +64:14:38.15. In the extended tracks we detect HS1700.850.1 in the synthesized image at  $\sim 16\sigma$ . The calibrated visibilities in the extended tracks were best fit by a single point source with an extracted flux density of  $S_{890\mu m}$  = 15.7 ± 1.1 mJy at a position of 17:01:17.779 and +64:14:37.85, consistent within 0.2" with the centroid of the 2mm continuum measurement from NOEMA. This is slightly offset to the south-west by 0.4" from the SMA compact track centroid. The extended SMA configuration may have partially resolved out fainter, more spatially extended  $850\mu m$  continuum emission which is seen in the compact configuration observations.

#### 2.3 Herschel SPIRE

We obtained *Herschel*-SPIRE observations for this field (Program ID OT2-ymatsuda-1) from the archive, with an integration time of 1.5 hr. We processed the images with the *Herschel* Interactive Processing Environment (HIPE; Ott 2010), following the standard data processing and map-making steps with destriping. The SPIRE FWHM is 18.1, 24.9, and 36.6 arcsec at 250, 350, and  $500\mu$ m, respectively. The bright source corresponding to HS1700.850.1 rises well above the confusion limit.

#### 2.4 Hubble Space Telescope

The Q1700 field was imaged with the *Hubble Space Telescope* (*HST*)/ACS using the F814W filter in program ID 10581, PI: Shapley (Peter et al. 2007). The total exposure time of 12,520 seconds corresponds to a sensitivity of 29.0 AB magnitude for a  $1\sigma$  surface brightness fluctuation in a 1" aperture, and a 28.4 AB magnitude depth for a  $10\sigma$  point source in a 0.1" radius circular aperture. The Multi Drizzle script (Koekemoer et al. 2002) was used to clean, sky-subtract, and drizzle the flat-fielded data products from the ACS CALACS software pipeline. The ACS image alignment to the IRAM frame was checked and refined using a nearby compact and well detected Distant Red Galaxy with a robust CO detection (Chapman et al. 2015a). The FWHM of the point-spread function of 0.12" corresponds to 1 kpc at z=2.8. All fluxes computed for HS1700.850.1 are tabulated in Table 1.

#### 3 RESULTS

# 3.1 Evidence in favour of a merger

The high resolution NOEMA data cube of HS1700.850.1 was analyzed to assess the source structure. An average CO line spectrum was measured for the total system by summing all pixels within the elliptical FWHM  $(1.3'' \times 0.7'')$ , PA=48 deg, East of North), yielding an optimal signal-to-noise ratio total spectrum. This 1D spectrum (Figure 1) is fully consistent with the integrated flux and properties tabulated for the lower spatial resolution double-peaked CO(5-4)

**Table 1.** Multi-wavelength fluxes for HS1700.850.1 (listed in mJy for continuum and Jy km s $^{-1}$  for lines, and AB-magnitude in the optical).

Wavelength	Red	Blue	Total	Instrument
F814W	26.7	25.4	25.1	HST
$250\mu\mathrm{m}$	_	_	$29.2 \pm 5.0$	Herschel
$350\mu\mathrm{m}$	_	_	$42.6 \pm 5.3$	Herschel
$450\mu\mathrm{m}$	_	_	$45 \pm 6$	SCUBA-2
$500\mu\mathrm{m}$	_	_	$30.0 \pm 6.4$	Herschel
$850\mu\mathrm{m}$	_	_	$18.2 \pm 1.1$	SCUBA-2
$870\mu\mathrm{m}$	_	_	$19.5 \pm 1.9$	SMA-COM
$870\mu\mathrm{m}$	_	$15.7 \pm 1.1$	_	SMA-EXT
2mm	_	_	$1.42 \pm 0.11$	NOEMA
3mm	_	_	$0.25 \pm 0.07$	NOEMA
I CO(5-4)	1.43±0.18	1.88±0.20	3.25±0.17	NOEMA

spectrum in Chapman et al. (2015b). The flux ratio of the two integrated peaks  $(1.31\pm0.30-\text{Table 1})$  is also in good agreement with the lower spatial resolution D-config data  $(1.23\pm0.15)$  from Chapman et al. (2015b) within errors. To assess the resolved structure, we first constructed intensity maps of each of the two clear CO velocity peaks (Figure 1), integrating all spectral channels within the FWHM of each of the peaks (FWHM  $\sim 0.86''$  and 0.98'' for the blue and red components, respectively.) The red and blue line intensity map centroids (defined as the pixel with the highest flux) show a clear spatial offset of  $0.73\pm0.17''$ , although the major axis of the  $0.8''\times0.4''$  naturally weighted beam has a position angle that is unfortunately aligned towards the separation axis of the red/blue components. This limits the interpretation of these offset components as disk or merger without performing further analysis.

We next assessed the optical morphology of the NOEMA-resolved structure using HST imagery in the F814W filter (~ I-band), or rest frame ultraviolet at z = 2.8. The blue and red NOEMA components are contoured over the HST image in Fig. 1 revealing a compact source near the blue NOEMA component and a diffuse and clumpy elongated structure near the red component. Their isophotal magnitudes, along with an integrated aperture magnitude of the entire system are reported in Table 1. There remains some astrometric uncertainty of ~ 0.3" between NOEMA and HST frames, although the global astrometry is consistent with the Spitzer IRAC detection centered on the combined blue/red sources in the low resolution CO detection presented in Chapman et al. (2015b). The distinct HST morphologies and alignment with the blue/red NOEMA components are consistent with a merger interpretation for this structure, although we caution that clumpy rest-ultraviolet morphologies are not uncommon in SMGs (Swinbank et al. 2010), with structured dust explaining the differences between the apparent counterparts of the NOEMA components. Figure 1 also shows the 870µm continuum map (SMA high resolution) overlaid on the blue/red CO intensity maps. Evident here is that the  $870\mu m$  emission is weighted more towards the blue CO component, suggesting it may have a larger dust mass (see § 3.4 for detailed analysis).

Next, we studied the kinematics of the structures through the CO line maps. We prepared the data cube for further analysis by fitting and subtracting the continuum measured in the off-line regions in each 0.13" pixel over the source. We then fit double Gaussians to all spectra measured in the source with integrated line flux detected above  $3\sigma$ . The total system is traced over 2.3" down to this  $3\sigma$  line flux limit, corresponding to 18.4 kpc. Examples of the continuum-subtracted spectra and Gaussian fits from our source are shown in Figure 2, while the total mosaic of all spectra >  $3\sigma$  is shown in the

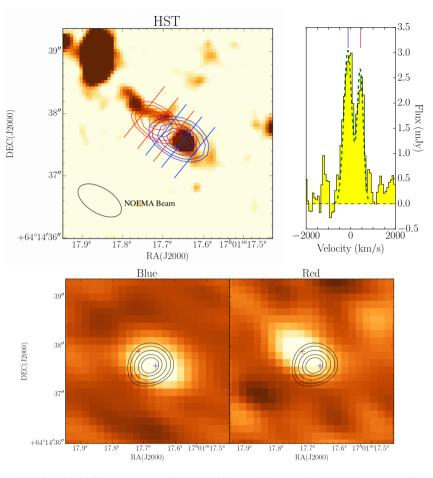


Figure 1. Top Left: Contours of the blue and red CO components of HS1700.850.1 overlaid on an HST F814W image, revealing compact optical emission near the blue component and a clumpy, elongated structure near the red component. The IRAC-NOEMA beam size is displayed in image, which has a position angle that is unfortunately aligned towards the separation axis of the red/blue components. The lines perpendicular to the major axis of the source show the position of the 1D spectra shown in Fig 2. The blue and red contours correspond to 90%, 80%, 70%, 60% and 50% of the max flux values for each component. **Top** Right: Average continuum subtracted, CO(5-4) one-dimensional spectrum taken over the FWHM ellipse of the full HS1700.850.1 system. The blue and red tick marks at the top of the plot correspond to the components' systemic redshifts, respectively. The zero velocity is defined as the midpoint of the total velocity spread for HS1700.850.1. **Bottom:** Relating the SMA 870 µm continuum to the CO: intensity maps in CO(5-4) of the HS1700.850.1 blue (**left**) and red (**right**) components are shown. The contours in the images display continuum maps at  $870\mu m$  from the SMA in extended configuration. Red and blue crosses indicate the centroid positions of the respective intensity maps. The contours correspond to 90%, 80%, 70%, 60% and 50% of the max flux values from the SMA map.

Appendix A. From the Gaussian fits, we then constructed velocity, dispersion and line intensity maps, also shown in Figure 2, and we highlighted the locations of the example extracted one-dimensional spectra with specific symbol markers. The velocity fields for each of the blue and red galaxy components show clear velocity gradients, with an offset in velocity of  $\sim 350 \text{ km s}^{-1}$  between the two components. This further suggests we are seeing a major merger between two gas rich disk galaxies. These line maps (Fig 2) also reveal some non-gaussian wings in some of the blue component line extractions (see § 3.5 for detailed analysis), suggesting again the blue component has distinct properties from the red.

To further characterize the structure, a position-velocity (PV) diagram of HS1700.850.1 was constructed (Figure 3) by slicing through the major axis of the integrated continuum source and plotting the velocity spectrum versus its position within the data. The diagram clearly reveals the two spatially separated sources with a clear break between the two sources where the map drops to the rms noise level, and the offset in velocity of  $\sim 350 \text{ km s}^{-1}$  is obvious. This configuration is not consistent with a single, large filled disk. The rotation fields derived from line fitting (Figure 2) are discernible in the PV diagrams for each component, with the blue source showing a larger spatial extent over the  $\sim 500 \text{ km s}^{-1}$  span of the velocity gradient.

Additional evidence for a merger comes from the integrated CO line profiles originally presented in Chapman et al. (2015b). We revisit this again, combining the new resolved CO(5-4) with the compact configuration observations in the image plane, resulting in similar line fluxes, but with substantially smaller (~40%) measurement errors (1.86±0.14 Jy km/s and 1.48±0.13 Jy km/s for the blue and red peaks respectively.) The  $^{12}$ CO J=5 to J=3 line ratios in the blue and red peaks then become 0.68±0.07 and 0.59±0.08, which now just agree within their  $1\sigma$  uncertainties.

However, these numbers belie the very different blue component line profiles between the J=5 and J=3 lines. Considering only the line peak values reveals a significantly stronger difference (30%) in the J=5 and J=3 line ratios. However, the blue component has a much broader  $\sigma_V$  in J=5 than it does at J=3, bringing  $R_{53}$  closer to the red component in the integrated lines.

We now understand these two velocity peaks to likely be two distinct merging galaxies, and so these differing line properties (line ratios and line widths) reflect differing conditions in the molecular

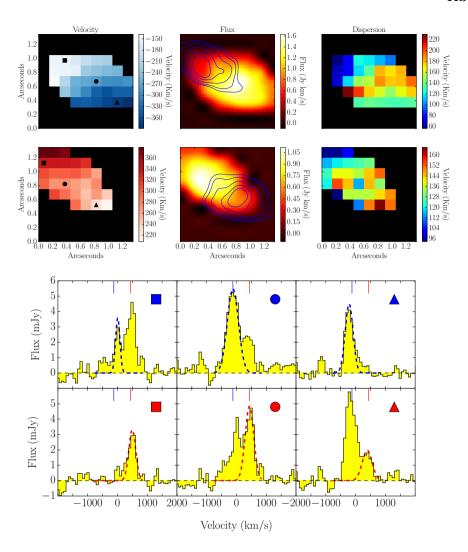


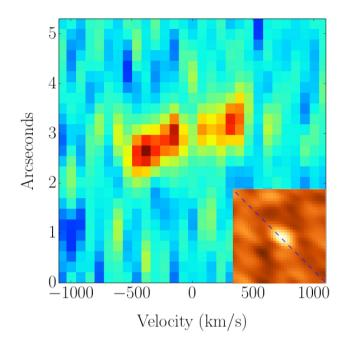
Figure 2. Top: The velocity, flux and dispersion maps were made from Gaussian line fitting for both the blue (top row) and red (bottom row) components (see text and Appendix B). The positions marked with symbols correspond to the pixel location of the 1D spectra below. The 1D spectra are labelled with the corresponding marker in their plots, whose locations are overlaid in Fig. 1 as well for reference. The flux maps also display the contours of the other respective component for reference. Only pixels with lines detected at  $> 4\sigma$  are displayed in these maps. Bottom: Representative 1D spectra and Gaussian fits at each of the source components' peak and edges. The marker displayed in the top right corner of each plot corresponds to the same symbol in the velocity map, showing the pixel location the spectra was extracted from. Fitted Gaussians are overlaid, colour-coded to the red or blue disk component to which they are referring. The blue and red tick marks at the top of the plot correspond to the components systemic redshifts, respectively.

gas of each galaxy. It would be hard to understand differing conditions in the opposite sides of a stable disk galaxy.

As a final critical piece of evidence for a merger, we point out that the detailed line properties in the blue and red components are very different. Most prominently, the velocity gradient in the blue component is more than 1.5× that of the red component (See Table 2), and the blue component shows more stability than the red component under the Toomre Q-parameter analysis (§ 3.3). The blue component also shows broad wings to the CO line, which are not seen in the red component (§ 3.4). If these CO line wings are due to a warping of the disk, they would offer further evidence that we are seeing two merging disk galaxies, with the warping of the wings being a direct consequence of the merger.

We therefore suggest that we have indeed resolved a merger in HS1700.850.1, based on eight pieces of circumstantial evidence: (i) The red and blue line channel map centroids show a clear spatial offset of  $0.73 \pm 0.17''$ ; (ii) The HST optical morphology shows two

distinct (and very different) components aligned to the red/blue CO components; (iii) The velocity fields for each of the blue and red galaxy components show clear velocity gradients, with an offset in velocity of 350 km s<sup>-1</sup> between the two components; (iv) A PV diagram reveals the two spatially separated sources with a clean break where the map drops to the rms noise level, inconsistent with a single, large filled disk; (v) Different gas conditions in the red and blue peaks ( $^{12}$ CO J=5 to J=3 integrated line ratios and line widths); (vi) The velocity gradient in the blue component is almost twice that of the red component, and the blue component shows more stability than the red component under the Toomre Q-parameter analysis (discussed in more detail in § 3.3); (vii) The  $870\mu m$  continuum emission appears to be more localized in the blue component, suggesting it has a larger dust mass (discussed further in § 3.4); (viii) The blue component shows broad wings to the CO line (Fig 2), which are not seen in the red component, possibly due to the interaction between the disks (discussed further in § 3.5).



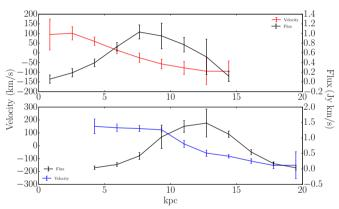


**Figure 3. Top:** The Position-Velocity (PV) diagram for HS1700.850.1, with an inset showing a  $5'' \times 5''$  cutout of the collapsed datacube (continuum plus line) and the dashed line showing the slice taken along the major axis of the galaxy in order to obtain the PV diagram. The slices are taken starting from the bottom right (blueshifted) to the top left (redshifted) of the cutout. **Bottom:** The rotation curves of each of the components (the blue and red curves, respectively for the blue shifted and redshifted CO(5-4) lines). The black curves show the CO(5-4) intensity profiles. The values were again taken along the disk major axis of the sources. Especially in the blue source, a characteristic disk velocity curve is traced, steepening through the core of the galaxy, and flattening at larger radii.

We analyze the properties of these two merging components in the following sections.

#### 3.2 Rotation curves and mass measurements

From the velocity maps, we constructed one-dimensional rotation curves for both the red and blue components (Figure 3) by slicing through the major axis of each source (defined by the maximum velocity spread) and extracting the peak velocity measurements recorded in each emission spectra. The CO(5–4) intensity profiles are also plotted for each source for reference. The errors shown are de-

rived from the line fitting uncertainty. The CO rotation curves of both components change relatively smoothly and monotonically between velocity extremes, however both show signs of flattening towards the edges of each curve. This would be expected if we were probing the dark matter halos beginning to dominate the mass profiles, although the result is only significant at  $> 3\sigma$  in the positive velocities of the blue component (and otherwise is consistent at  $\sim 2\sigma$  with no flattening).

We next use these rotation curves to estimate the disk masses. In this case, the dynamical mass is given by,

$$M_{\rm dyn} < \sin^2(i) > [M_{\odot}] = 2.35 \times 10^5 V^2 R$$
 (1)

where V is the line of sight circular velocity in km s<sup>-1</sup>, R is in kpc, and i is the inclination of the galaxy. For our calculations, V has already been calculated as the velocity gradient, and the R used is the Half Width Half Maximum of the intensity profiles in Figure 3. We adopt a mean inclination angle, suitable for a collection of randomly oriented disks of  $<\sin(i)>=\pi/4\simeq0.79$  (see Law et al. 2009). Using this rotational estimate, the dynamical mass for the blue and red components of HS1700.850.1 are  $(1.5 \pm 0.2) \times 10^{11}$  M $_{\odot}$  and  $(0.71 \pm 0.22) \times 10^{11}$  M $_{\odot}$  respectively. It is worth noting that if the inclination of these galaxies is closer to an edge on view (smaller i) then the dynamical mass is being underestimated by our calculations. Conversely, if the inclination is more face on (larger i) then these estimates are larger than their actual by a factor of  $\sim 1.6$ .

We can also compare these individual component dynamical masses with an estimate of the total halo mass, by taking the systemic velocity of each of the disks and applying the virial theorem with the velocity separation of the two components as input (e.g., Swinbank et al. 2006). Using equation 1, the mass of the total system is  $(16 \pm 2) \times 10^{11} \ M_{\odot}$ , nearly eight times the summed mass of the two components, although we note this comparison does depend upon the inclination of each galaxy and their orbit. Since this halo mass estimate only includes the line of sight velocity component and their projected separation, the actual halo mass could be higher than this.

#### 3.3 Stability of HS1700.850.1

To further quantify the structure of this source, we look at Toomre's Q criterion, which characterizes the stability of a gas rich disk against local axisymmetric perturbations. In order for a galaxy to be stable it must have a Q > 1, otherwise it will fragment and collapse into giant dense clumps. The Toomre parameter is calculated from

$$Q = \frac{\sigma_{r \kappa}}{\pi G \Sigma_{\text{gas}}} \tag{2}$$

where  $\kappa$  is the epicyclic frequency,  $\sigma_r$  is the line of sight velocity dispersion, and  $\Sigma_{\rm gas}$  is the mass surface density of the gas (Toomre 1964). Here we have adopted  $\kappa = aV_{\rm max}/r$  which is appropriate for a uniform disk, where  $(a=\sqrt{3})$ , and we have assumed that the measured velocity dispersion is equal to  $\sigma_r$ . By estimating  $\Sigma_{\rm gas}$ , we derive  $Q=1.50\pm0.20$  and  $1.20\pm0.18$  for the blue and red disk components respectively. These are similar to typical Q values for gas rich star forming galaxies at  $z{\sim}2$  (Genzel et al. 2014), and indicate that both disks are still very stable despite the ongoing merger. The dynamical mass ratio estimate for the merging components equates to  $0.47\pm0.12$ . This is consistent with being a major merger (which have mass ratios of 1:3 or closer to unity; eg., Bothwell et al. 2010; Engel et al. 2010). The lack of a highly turbulent component (small measured  $\sigma_r$  for the  $V_{\rm max}$ ) may indicate the galaxies are being found at their first approach.

#### 3.4 Continuum properties and SFRs

We next attempt to constrain the rest-frame far infrared continuum properties of the red and blue galaxy components, in order to better estimate their SFRs. The 2mm continuum map from NOEMA does not significantly resolve the two components, due to the position angle of the synthesized beam lying near the merger axis of the components. Intensity maps of both the blue and red CO components of HS1700.850.1 can be seen in Figure 1 with the extended configuration  $870\mu m$  imaging contoured over top. The offset of the  $870\mu m$  centroid to the blue component centroid is  $0.22'' \pm 0.08''$ , compared to that of the red component,  $0.51'' \pm 0.12''$ . These results were obtained by combining the beam uncertainties (as the beam<sub>FWHM</sub>/SNR) at both wavelengths in quadrature. The  $850\mu m$  continuum is better aligned with the blue galaxy component, suggesting that this component may carry a majority of the  $850\mu m$  flux.

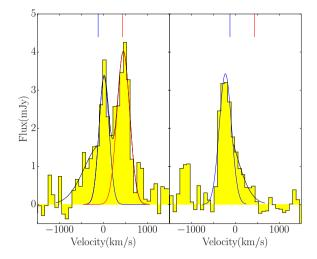
We next fit a Spectral Energy Distribution (SED) template from the Dale et al. (2005) library to the integrated continuum measurements of the source using *Herschel*-SPIRE, compact configuration SMA, and compact configuration NOEMA measurements. The temperature of the template is increased until the  $\chi^2$  with the photometry is minimized, resulting in an SED of  $T_d$ =36.1±3.1 K. This is comparable to the average  $T_d$  measured by Chapman et al. (2010) and Magnelli et al. (2014) for SMGs followed up with SPIRE, as well as Swinbank et al. (2014) for a large sample of field SMGs using ALMA fluxes with deconvolved constraints on the SED peak from SPIRE. Given the uncertainty in  $T_d$ , our new estimate for the  $L_{IR}$ =4.3±1.4  $\times$  10 $^{13}$   $L_{\odot}$  is not appreciably different from that estimated previously (without the SPIRE photometry) of 3.8×10 $^{13}$   $L_{\odot}$  (Chapman et al. 2015b). Based on the scaling relations mentioned in Birkin et al. (2021), the dust mass of the total system would then be  $M_{dust}$ =3.2  $\times$  10 $^9$ .

While we cannot unambiguously resolve the continuum in the two components, and thus cannot reasonably infer individual  $L_{IR}$  from SED modelling, the weighting of the  $870\mu m$  emission centroid towards the blue component is consistent with the CO(3-2) luminosity of the blue component being  $1.4\times$  higher than that of the red component. A corresponding division of the total SFR (3800±600  $M_{\odot}$  yr $^{-1}$ ) by the same ratio would yield 2216±500 and 1583±300  $M_{\odot}$  yr $^{-1}$  respectively for the blue and red components.

#### 3.5 Potential wings to the CO lines

The full line map of the merging complex (shown in Appendix-A) was also studied pixel by pixel for any features or irregularities in line profiles. Upon detailed inspection of the CO(5-4) spectra, the more massive (blue) component appears to show wings in the emission extending to velocities  $\sim \pm 1000\, {\rm km\, s^{-1}}$  from systemic. The wings are only discernible in the off-nuclear regions, spatially offset by  $\sim 4.0\, {\rm kpc}$  in each direction along the major axis from the disk centroid. An example of such spectra can be seen in Figure 4, which shows the highest significance spectra positions in the North-East and South-West regions. The full spectral maps shown in Appendix-A confirm visually that the central pixels do not exhibit any significant wings to the line.

These wings are more prominent in the North-East region, and can be cleanly isolated here as a velocity channel map. Figure 4 shows the channel map for this low velocity wing, defined between the range of -800kms to -450km/s, well outside the full-width zero intensity regime of the blue line. The blue components integrated channel map is contoured over the wing map, which clearly shows a spatial offset of 0.4'' from galaxy centroid to the extended line wing region. It is more difficult to construct a similar channel map of the



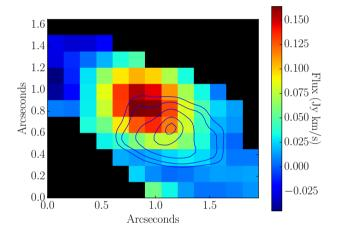


Figure 4. A potential warp (or outflow) in the blue galaxy's gas disk – Top Left: A spectral region spanning  $\sim 0.3''$  found in the North-East section of the blue disk galaxy, with a clear wing on the blue side of the blue peak. The blue and red tick marks at the top of the plot correspond to the components systemic redshifts, respectively. Top Right: Similarly, a spectral region found in the South-West component of the blue source, with again, a wing on the side of the peak. The blue and red tick marks at the top of the plot correspond to the components systemic redshifts, respectively. Bottom: The integrated channel map of the wing (defined as  $-800 \, \text{km/s}$  to  $-450 \, \text{km/s}$ ) that appears in the North-East region of the blue galaxy. The contours display the integrated channel map of the blue source, which shows a clear spatial offset with the wing and the blue galaxy by 0.5'', well outside the full-width zero intensity regime of the blue line.

weaker positive velocity wing in the South-West, but it is clear from the emission line spectra that it exhibits a similar offset from the galaxy centroid.

These wings could be interpreted as a warping of the gas disk from tidal forces, tidal features due to the merger (Barnes 2002) or even faint satellite galaxies around the blue component. However wings on CO lines have also been interpreted as outflowing gas (Maiolino et al. 2012). The lack of wings on the CO line in the core region might be more consistent with such a *disk warp* interpretation. However, an episodic outflow driven by star formation or an Active Galactic Nucleus (AGN) could launch material out of the disk resulting in its

detection only in these off-center locations (e.g., Cicone et al. 2015). In § 4.2 we assess these wings under these various possibilities.

#### 4 DISCUSSION

#### 4.1 Star formation in two massive disks

We have demonstrated that HS1700.850.1 is likely to represent two CO gas-rich disks undergoing a merger. The merger itself is likely responsible for substantially elevating the far-infrared luminosity (and hence SFR) to high levels. The very typical dust temperature  $(T_d=36.1\pm3.1 \text{ K})$  we have constrained for the system as a whole suggests that a large dust masses is associated with the galaxies (via the large 850 $\mu$ m flux). A gas mass ratio of the components of 1.4× is estimated from the Gaussian fits to the CO(3–2) peaks (Chapman et al. 2015b). With the majority of the  $850\mu m$  flux attributed to the blue component (in a ratio potentially as high as  $\sim 3\times$ ), the dust mass of the blue component may be substantially higher than the red. However, differences in dust temperature can affect this estimate - the difference in T<sub>d</sub> would have to be about a factor of two to bring the dust mass ratio in line with the gas mass ratio between components (assuming two thirds of the  $850\mu$ m emission was associated with the blue component).

Major mergers are often invoked to explain very high SFR bursts, although there are counterexamples. Engel et al. (2010) concluded, based on high-resolution CO imaging, that  $z\sim2$  SMGs are typically nuclear starbursts on scales < 4 kpc, driven by major gas-rich mergers, and hypothesize that mergers must be the driving mechanism behind the high SFRs. However there have since been studies of SMGs that suggest that mergers are not necessary to trigger the starbursts, for instance Gullberg et al. (2019). Narayanan et al. (2008) simulated a massive gas rich merger as the only plausible route to generating a SFR consistent with the S<sub>850 $\mu$ m</sub> ~20 mJy SMG, GN20 (Pope et al. 2006). However, high resolution followup of GN20 revealed a large undisturbed disk galaxy with no signs of mergers (Hodge et al. 2012). Davé et al. (2010) suggest that a substantial fraction of SMGs could be fed primarily by a cold mode accretion (e.g., Dekel et al. 2009a; Kereš et al. 2009) and not major mergers.

Another question is whether HS1700.850.1 is on its first approach, or has already gone through a close encounter. While relatively ordered rotation is observed in the extended gas distributions, the extended CO wings in the blue component (§ 3.4) suggest tidal forces at work. HS1700.850.1 has a projected separation of 8 kpc between the two massive disk components. The simulations in Narayanan et al. (2015) suggest that the SFRs of the disks may not be elevated by more than ~20% from tidal forces in the interaction if this is a first approach. Further, comparison to these simulations suggests that our measured CO rotation out to ~5 kpc radius is not particularly unusual in these massive systems. If we consider only the half-light size, from the exponential fit to the CO line intensity, the CO disk radius is 6 kpc, in the upper third of massive systems considered in Narayanan et al. (2015). The gas distributions and velocity fields (Figures 1&2) of the disks in HS1700.850.1 are also qualitatively similar to that seen in the simulated SMG maps of Davé et al. (2010) though the SFRs of these simulated galaxies are substantially lower than HS1700.850.1. Carilli et al. (2010) and Hodge et al. (2012) used arguments of ordered disk-like gas motions to claim no major merger origin to the z = 4.05 GN20 submm galaxy. However, such signatures do not conclusively rule out a merger, as Robertson & Bullock (2008) have shown that ordered rotation of an extended gas disk can be reestablished very shortly after a major merger. It is possible that

**Table 2.** Derived properties of the individual red and blue components of HS1700.850.1. For the SFR, the estimates are based on the CO luminosity ratio applied to the total measured SFR from § 3.4. The integrated stellar mass was calculated in Chapman et al. (2015b) from a hyper-z fit to the IRAC and near-IR photometry. The final column presents either the sum of the two components (total), or the value derived from the combined or integrated system.

	Red	Blue	Total/Combined
$V_{p-p} (km s^{-1})$	196±13	303±15	854±42
$\sigma$ (km s <sup>-1</sup> )	136±33	180±39	375±54
Q	$1.20 \pm 0.18$	$1.50 \pm 0.20$	-
SFR $(M_{\odot} \text{ s}^{-1})$	1600±300	2200±500	3800±600
$M_{gas} (M_{\odot})$	$7.0\pm1.1\times10^{10}$	$10.1\pm1.2\times10^{10}$	$17.5\pm1.4\times10^{10}$
$M_* (M_{\odot})$	_	_	$5.8 \pm 1.5 \times 10^{10}$
$M_{dyn}\;(M_{\odot})$	$0.71\pm0.22\times10^{11}$	$1.5\pm0.2\times10^{11}$	$16 \pm 2 \times 10^{11}$

the HS1700.850.1 component galaxies have already interacted with each other in a close encounter, but quickly reestablished their disk morphologies on a timescale shorter than the dynamical time > 6kpc / 550 km s $^{-1}$  or  $\simeq \! 11$  Myr.

#### 4.2 Interpreting the CO line wings in the blue component

The CO line wings in the HS1700.850.1 blue component are intriguing. Given that a major merger has been characterized with a variety of evidence (§ 3.1), the wings may well be further evidence for the merger in the form of tidal warping of the gaseous disk. Most indicative, we see the line wings only at the edges of the disk (more susceptible to the torques from the merger) and not in the center.

Barnes (2002) presented early evidence from simulations that mergers of massive disk galaxies can lead to strong and persistent tidal features in the gaseous and stellar components of the disks. In a series of N-body experiments with merging massive galaxies, showing a range of pattern speeds, Dubinski & Chakrabarty (2009), found that the torques from the merger are strong enough to induce long-lived transient warps in the disks. These would appear similar to our CO wings found in HS1700.850.1, and with a similar luminosity ratio to the unwarped disk (with luminosity interpreted as molecular gas mass). Even without a direct merger, strong warps are possible to the disks by nearby interactions. Kim et al. (2014) used N-body simulations to investigate the morphological and kinematical evolution of disks when galaxies undergo flyby interactions with adjacent dark matter halos, and found similar warping is possible. With direct observations in the nearby LIRGs, NGC 3110 and NGC 232, Espada et al. (2018) showed very similar warping behaviour to the CO(2-1) lines from an SMA study of these merging disk galaxies.

A key question however is why other SMGs in this luminosity class do not typically exhibit the broad CO-line wings found in the blue component of HS1700.850.1? By comparison to the lower resolution data, it is clear that these faint wings only emerge through a careful high resolution analysis of the outer regions of the velocity field of the blue disk, and is not discernable in the lower spatial resolution data (Chapman et al. 2015b) or in the integrated line properties of the merging system. It is thus possible that other SMGs studied in detail at high resolution may show similar features.

Another possible interpretation of the broad wings on the CO lines is a molecular outflow. We view this as less likely as if they're winds then we should see them across the disk, whereas no extended line profile is seen in the core of the galaxy. This would be possible if the

winds were launched in the past and we are currently seeing them shut off (Cicone et al. 2015), but is somewhat contrived given the immense ongoing starburst. For completeness we assess the basic properties of the emission line wings, assuming it is an outflow. Since we are unaware of the geometry of HS1700.850.1, we adopt a simple model following the arguments of Maiolino et al. (2012), where the outflow occurs in a spherical volume with radius  $R_{\text{outfl}}$  which is uniformly filled with outflowing gas:

$$\dot{M}_{outfl} \approx v \Omega R_{outfl}^2 \langle \rho_{outfl} \rangle v = 3 v \frac{M_{outfl}}{R_{outfl}}$$
 (3)

where  $\nu$  is the outflow velocity,  $\Omega$  is the total solid angle subtended by the outflow, and  $\rho_{\rm outfl}$  is the volume averaged density of the gas in the outflow.  $M_{\rm outfl}$  was calculated by determining the  $L'{\rm CO}$  given its relationship to  $M_{\rm gas}$ , assuming an  $\alpha=1$ . (Solomon & Vanden Bout 2005.) An average CO flux (0.43 Jy km s<sup>-1</sup>) was estimated with aperture photometry over the CO wing channels, yielding a total mass of the outflow of  $1.99 \times 10^{10} {\rm M}_{\odot}$ .

Again following the arguments of Maiolino et al. (2012), the radius of the outflow is measured as 4.0 kpc from the map in Figure 4, multiplying by 2 to account for matter ejected towards the outside of the galaxy. The velocity of the outflow is estimated to be the maximum value observed of 600 km s<sup>-1</sup>. Given this, the outflow rate was calculated to be  $\dot{M}_{outfl} > 4590 \text{ M}_{\odot} \text{ yr}^{-1}$ . We also note that if instead we assumed a shell like geometry, the outflow rate would be even higher. The lower limit on the outflow rate is then comparable to the SFR (2500  $\ensuremath{M_{\odot}}\xspace$  yr^-1) of the blue disk galaxy, and hence quenching star formation within less than 20 Myr (assuming a constant outflow rate with no new supply of gas from the outside.) This interpretation of the wings on the CO lines provides an extreme outflow scenario compared to the literature, although consistent with expected scaling relations. The lack of any evidence for an AGN from X-ray and infrared SED (Chapman et al. 2015b) suggests that any outflow if real might be driven entirely by the copious star formation in the blue galaxy component.

# **4.3 The environment of** HS1700.850.1

Our deep (sub)mm-wave maps provide a route to searching for faint companions that may have gone unnoticed previously in submm studies of this field. However no additional continuum sources were significantly detected in our combined SMA 870 $\mu$ m map reaching 0.9 mJy rms (§ 2.2). The combined A+D config 2mm continuum map from NOEMA is also substantially deeper than the D-config map presented in Chapman et al. (2015b). We searched the deconvolved map for additional point sources, but found none to a limit of  $5\sigma$  of 0.25 mJy (§ 2.1). We searched the full data cube over the 7000 km s<sup>-1</sup> probed by the WIDEX correlator band for any additional CO line candidates. We found no sources at >  $5\sigma$  significance with kernels ranging from 200-1000 km s<sup>-1</sup>.

Thus aside from the on-going merger we have resolved with these new observations, there is no additional evidence for a locally overdense surrounding environment for HS1700.850.1. As previously discussed, HS1700.850.1 appears to reside in a relative void in the LBG redshift distribution of this field (Chapman et al. 2015b), with no known companion UV-selected galaxies within  $dz \sim 0.05$  and 3' (1.44 Mpc proper) radius.

In line with not living in an overdense environment, and by analogy with Hyperluminous quasars which have good statistical measurements of their environment (Trainor & Steidel 2012), the expected halo mass of HS1700.850.1 should be no greater than  $\sim 10^{13}~M_{\odot}$ . Our dynamical measurement of the merging pair (§3.2) puts a lower

limit on the mass of  $1.6 \pm 0.2 \times 10^{12} \, \mathrm{M_{\odot}}$ , and comparison to other studies suggests this is also a typical mass for the observed velocity separations of massive SMGs (e.g. Swinbank et al. 2006.)

## 4.4 The properties of the most luminous SMGs

We next compare the properties of HS1700.850.1 to other SMGs with comparably bright  $850\mu m$  luminosities. Sources such as HS1700.850.1 remain very rare in surveys. ALMA and SMA followup to sources from the SCUBA-2 Cosmology Legacy Survey (S2CLS – Geach et al. 2017) presents the best benchmark for comparison. Only three sources with a single ALMA or SMA component S<sub>850 $\mu m$ </sub> >19mJy exist in the ~5deg<sup>2</sup> of the S2CLS, while only eight more such sources with S<sub>850 $\mu m$ </sub> >15mJy are identified.

Specifically, in the SMA followup of GOODS-N by Barger et al. (2014), one source was found  $S_{850\mu m} > 19 \text{mJy}$  (the well studied GN20 – Hodge et al. 2012), and one was found  $S_{850\mu m} > 15 \text{mJy}$ . From the other northern S2CLS fields (AEGIS, SSA22, and Lockman), Hill et al. (2018) used the SMA in compact configuration to followup all the brightest  $850\mu m$  sources > 8 mJy, and after deboosting, identified two SMGs with  $S_{850\mu m} > 15 \text{mJy}$ , both in the AEGIS field.

Stach et al. (2018) did not find any sources with  $S_{850\mu m} > 15 \text{mJy}$  in the ALMA follow up of the  $1.6 \text{ deg}^2$  UDS field. There is a 30mJy source in the field, but it has been characterized as gravitationally lensed (Ikarashi et al. 2015) and was not revisited in Stach et al. (2018). Simpson et al. (2020) used ALMA to follow up the 180 brightest sources in the COSMOS field  $(1.6 \text{ deg}^2)$ , finding 10 with peak  $S_{850\mu m} > 15 \text{mJy}$  and two with  $S_{850\mu m} > 19 \text{mJy}$ . After deboosting, this becomes six sources with  $S_{850\mu m} > 15 \text{mJy}$ , only one of which has  $S_{850\mu m} > 19 \text{mJy}$ .

Clearly these hyper-luminous submm sources show a great deal of cosmic variance. However, the statistics support our uncovering of HS1700.850.1 in ~0.3 deg<sup>2</sup> of the KBSS followup as in line with these S2CLS surveys. Our extended configuration SMA results suggest that the blue component of HS1700.850.1 may carry the majority (~15 mJy) of the 19.5mJy 870 $\mu$ m flux measured in the larger beam compact configuration observations. Our comparison sample could therefore be 11 sources in 5 deg<sup>2</sup>. However the SMA followup discussed above would not distinguish HS1700.850.1 as two individual galaxies, and 3 in 5 deg<sup>2</sup> remains a plausible statistic to compare.

Comparing some of the brightest SMGs that have been similarly characterized kinematically can provide some context to HS1700.850.1. Another very bright source initially found from *Herschel* surveys (SGP38326 at z=4.425, with S<sub>850 $\mu$ m</sub>=23 mJy – Oteo et al. 2016) is clearly characterized by a major merger, similar to HS1700.850.1, supporting gas-rich mergers as a means to trigger such immense luminosities. Narayanan et al. (2009) used hydrodynamical simulations to highlight the final stage merger of two extremely gas rich, massive disk galaxies as a likely trigger of similarly intense starbursts.

Several studies have predicted that mergers configured with counter-rotating gas disks should lead to the most intense starbursts (e.g. Mihos & Hernquist 1994, 1996; Taniguchi & Shioya 1998; Borne et al. 2000; Bekki (2001); Di Matteo et al. 2007; Salomé et al. 2012). Although the components within SGP38326 (Oteo et al. 2016) are resolved into counter-rotating gas disks, HS1700.850.1 appears to resolve into two co-rotating disks, presenting a possible counterexample to the above studies. However we do not robustly constrain the inclination angle of the disks in HS1700.850.1, and they may still

represent a merger quite far from co-rotating but seen in projection as roughly co-rotating.

Other hyper-luminous SMGs do not show obvious signs of a major merger. Of all the bright SMGs noted above in the S2CLS fields, only GN20 (z=4.055) has been studied at sufficiently high-resolution to compare to HS1700.850.1. High resolution followup in <sup>12</sup>CO by Hodge et al. (2012) has demonstrated that GN20 exhibits highly symmetrical disk-like kinematics in its gaseous components. This is similar to another bright source found from Herschel surveys, SMM J084933 at z=2.410 (Ivison et al. 2013). While apparently not involved in a major merger, these bright SMGs both signpost large overdensities of galaxies, suggesting dense environments remain an important trigger of such luminous activity. The gas disk in these cases may have recently reformed around the joint system. Simulations in Narayanan et al. (2015) suggest that while the brightest SMGs are composed of multiple sources, the most active submm phase is often associated with a relatively isolated period, several hundred Myrs after the most recent major merger. It is possible that GN20 and J084933 are consistent with this picture.

## **5 CONCLUSIONS**

We have presented a high spatial resolution spectral analysis of the HyLIRG HS1700.850.1, the brightest  $850\mu$ m source found in the SCUBA-2 KBSS fields.

- We have resolved the CO emission into two components, which exhibit the expected properties of merging galaxies. This is supported by at least eight corroborating pieces of evidence (§ 3.1). Some of the stronger evidence includes the gap in the velocity field (which would otherwise require a central hole in the gas disk), and a range of differences in properties of the blue and red components. The  $R_{53}$  CO line ratio differences for instance would otherwise imply an inhomogeneous ISM within the system if it were a single large disk rather than two merging disks. Differing dust/gas masses, velocity gradients, and stability analysis within the two components are also difficult to explain in a single large rotating system.
- Each component of the merger shows well ordered gas motions of a massive, but turbulent disk. The CO rotation curve of the blue disk shows some evidence for flattening of the rotation profile.
- As we have resolved the size of each of the disks beyond the beam (0.8" beam size along the rotation axis), the 0.4" FWHM of the beam minor axis puts a strong constraint on the inclination of each of the disks, and removes some of the  $\sin(i)$  uncertainty in the mass estimates from rotation. We estimate disk masses of the blue and red components, finding that they are of order  $10^{11} \, \mathrm{M}_{\odot}$ .
- The more massive (blue) component shows extended wings in CO(5–4) due to either a warp/tidal feature, or less likely a molecular outflow in the gas disk.

A number of key observations are required to untangle the mechanisms driving star formation in HS1700.850.1. Higher-resolution imaging of the millimeter continuum would better reveal the distribution of star formation across the disk in greater detail. While our NOEMA and SMA continuum measurements have resolved the two merging disks separated by only 0.7", the beamsizes are comparable to the separation. Higher-resolution imaging of low-*J* and high-*J* CO transitions can be used to determine the spatial excitation of the molecular gas, which will be possible with recent and upcoming baseline increases at NOEMA. Our observations have succeeded in resolving the gas beyond the beam in each disk, showing clear rotation patterns. However the internal excitation of the gas in the disks have yet to be determined, requiring more than one CO transition.

Shapiro et al. (2008) show that with such resolved measurements, the higher order *kinemetry* of the line maps can further enable an empirical differentiation between merging and non-merging galaxies.

We have thus been able to substantially increase our detailed understanding of this hyper-luminous SMG. Such sources remain very rare – only three comparably bright  $S_{850\mu m} > 19 \text{mJy}$  sources exist in the ~5deg² of the S2CLS Legacy survey, followed up with ALMA and SMA, while only eight more sources with  $S_{850\mu m} > 15 \text{ mJy}$  are identified. Comparing some of the brightest SMGs that have been similarly characterized kinematically, we find they often show explicit signs for being in a merger, or else are signposting a massive overdensity of galaxies, indicating that recent mergers were likely and abundant gas supplies feeding the SMG are likely present. HS1700.850.1, despite being in an active merger, remains somewhat unique in the literature of hyper-luminous SMGs, in residing in such a rarefied environment lacking submm companions or an overdensity of galaxies at the same redshift.

#### **ACKNOWLEDGEMENTS**

This work is based on observations carried out under project number S17BS with the IRAM NOEMA Interferometer. IRAM is supported by INSU/CNRS (France), MPG (Germany) and IGN (Spain). The Submillimeter Array is a joint project between the Smithsonian Astrophysical Observatory and the Academia Sinica Institute of Astronomy and Astrophysics and is funded by the Smithsonian Institution and the Academia Sinica. SC acknowledges support from NSERC and CFI. IRS acknowledges support from STFC (ST/T000244/1).

#### DATA AVAILABILITY STATEMENT

The data underlying this article will be shared on reasonable request to the author.

Barger A. J., Cowie L. L., Sanders D. B., Fulton E., Taniguchi Y., Sato Y.,

#### REFERENCES

```
Kawara K., Okuda H., 1998, Nature, 394, 248
Barger A. J., et al., 2014, ApJ, 784, 9
Barnes J. E., 2002, MNRAS, 333, 481
Barnes J. E., Hernquist L., 1996, ApJ, 471, 115
Bekki K., 2001, ApJ, 546, 189
Birkin J. E., et al., 2021, MNRAS, 501, 3926
Borne K. D., Bushouse H., Lucas R. A., Colina L., 2000, ApJ, 529, L77
Bothwell M. S., et al., 2010, MNRAS, 405, 219
Bryant P. M., Scoville N. Z., 1999, AJ, 117, 2632
Carilli C. L., et al., 2010, ApJ, 714, 1407
Chapman S. C., Blain A. W., Ivison R. J., Smail I. R., 2003a, Nature, 422,
Chapman S. C., Windhorst R., Odewahn S., Yan H., Conselice C., 2003b,
    ApJ, 599, 92
Chapman S. C., Blain A. W., Smail I., Ivison R. J., 2005, ApJ, 622, 772
Chapman S. C., et al., 2010, MNRAS, 409, L13
Chapman S. C., et al., 2015a, MNRAS, 449, L68
Chapman S. C., et al., 2015b, MNRAS, 453, 951
Cicone C., et al., 2015, A&A, 574, A14
Dale D. A., et al., 2005, ApJ, 633, 857
Davé R., Finlator K., Oppenheimer B. D., Fardal M., Katz N., Kereš D.,
    Weinberg D. H., 2010, MNRAS, 404, 1355
Dekel A., et al., 2009a, Nature, 457, 451
Dekel A., Sari R., Ceverino D., 2009b, ApJ, 703, 785
```

Di Matteo P., Combes F., Melchior A. L., Semelin B., 2007, A&A, 468, 61

```
Downes D., Solomon P. M., 1998, ApJ, 507, 615
Dubinski J., Chakrabarty D., 2009, ApJ, 703, 2068
Dudzevičiūtė U., et al., 2020, MNRAS, 494, 3828
Elmegreen D. M., Elmegreen B. G., 2006, ApJ, 651, 676
Elmegreen B. G., Elmegreen D. M., Fernand ez M. X., Lemonias J. J., 2009,
    ApJ, 692, 12
Engel H., et al., 2010, ApJ, 724, 233
Espada D., et al., 2018, ApJ, 866, 77
Fardal M. A., Katz N., Gardner J. P., Hernquist L., Weinberg D. H., Davé R.,
    2001, ApJ, 562, 605
Finlator K., Davé R., Papovich C., Hernquist L., 2006, ApJ, 639, 672
Förster Schreiber N. M., et al., 2006, ApJ, 645, 1062
Förster Schreiber N. M., et al., 2009, ApJ, 706, 1364
Geach J. E., et al., 2017, MNRAS, 465, 1789
Genzel R., et al., 2008, ApJ, 687, 59
Genzel R., et al., 2014, ApJ, 785, 75
González J. E., Lacey C. G., Baugh C. M., Frenk C. S., 2011, MNRAS, 413,
Gullberg B., et al., 2019, MNRAS, 490, 4956
Hayward C. C., Kereš D., Jonsson P., Narayanan D., Cox T. J., Hernquist L.,
    2011, ApJ, 743, 159
Hayward C. C., Jonsson P., Kereš D., Magnelli B., Hernquist L., Cox T. J.,
    2012, MNRAS, 424, 951
Hill R., et al., 2018, MNRAS, 477, 2042
Hill R., et al., 2019, MNRAS, 485, 753
Hodge J. A., da Cunha E., 2020, Royal Society Open Science, 7, 200556
Hodge J. A., Carilli C. L., Walter F., de Blok W. J. G., Riechers D., Daddi E.,
    Lentati L., 2012, ApJ, 760, 11
Hughes D. H., et al., 1998, Nature, 394, 241
Ikarashi S., et al., 2015, ApJ, 810, 133
Ivison R. J., Papadopoulos P. P., Smail I., Greve T. R., Thomson A. P., Xilouris
    E. M., Chapman S. C., 2011, MNRAS, 412, 1913
Ivison R. J., et al., 2013, ApJ, 772, 137
Kereš D., Katz N., Weinberg D. H., Davé R., 2005, MNRAS, 363, 2
Kereš D., Katz N., Fardal M., Davé R., Weinberg D. H., 2009, MNRAS, 395,
    160
Kim J. H., Peirani S., Kim S., Ann H. B., An S.-H., Yoon S.-J., 2014, ApJ,
    789, 90
Koekemoer A. M., et al., 2002, ApJ, 567, 657
Lacaille K. M., et al., 2019, MNRAS, 488, 1790
Law D. R., Steidel C. C., Erb D. K., Larkin J. E., Pettini M., Shapley A. E.,
    Wright S. A., 2009, ApJ, 697, 2057
Magnelli B., et al., 2014, A&A, 561, A86
Maiolino R., et al., 2012, MNRAS, 425, L66
McAlpine S., et al., 2019, MNRAS, 488, 2440
Michałowski M. J., et al., 2017, MNRAS, 469, 492
Mihos J. C., Hernquist L., 1994, ApJ, 431, L9
Mihos J. C., Hernquist L., 1996, ApJ, 464, 641
Narayanan D., Cox T. J., Shirley Y., Davé R., Hernquist L., Walker C. K.,
    2008, ApJ, 684, 996
Narayanan D., Cox T. J., Hayward C. C., Younger J. D., Hernquist L., 2009,
    MNRAS, 400, 1919
Narayanan D., Hayward C. C., Cox T. J., Hernquist L., Jonsson P., Younger
    J. D., Groves B., 2010, MNRAS, 401, 1613
Narayanan D., et al., 2015, Nature, 525, 496
Oteo I., et al., 2016, ApJ, 827, 34
Ott S., 2010, in Mizumoto Y., Morita K. I., Ohishi M., eds, Astronom-
    ical Society of the Pacific Conference Series Vol. 434, Astronomical
    Data Analysis Software and Systems XIX. p. 139 (arXiv:1011.1209),
    doi:10.48550/arXiv.1011.1209
Peter A. H. G., Shapley A. E., Law D. R., Steidel C. C., Erb D. K., Reddy
    N. A., Pettini M., 2007, ApJ, 668, 23
Pope A., et al., 2006, MNRAS, 370, 1185
Riechers D. A., Hodge J., Walter F., Carilli C. L., Bertoldi F., 2011, ApJ, 739,
Robertson B. E., Bullock J. S., 2008, ApJ, 685, L27
```

Rudie G. C., et al., 2012, ApJ, 750, 67

```
Salomé P., Guélin M., Downes D., Cox P., Guilloteau S., Omont A., Gavazzi
    R., Neri R., 2012, A&A, 545, A57
Scoville N. Z., Carlstrom J. E., Chandler C. J., Phillips J. A., Scott S. L.,
    Tilanus R. P. J., Wang Z., 1993, PASP, 105, 1482
Shapiro K. L., et al., 2008, ApJ, 682, 231
Simpson J. M., et al., 2014, ApJ, 788, 125
Simpson J. M., et al., 2015, ApJ, 799, 81
Simpson J. M., et al., 2020, MNRAS, 495, 3409
Smail I., Ivison R. J., Blain A. W., 1997, ApJ, 490, L5
Solomon P. M., Vanden Bout P. A., 2005, ARA&A, 43, 677
Stach S. M., et al., 2018, ApJ, 860, 161
Steidel C. C., Adelberger K. L., Shapley A. E., Erb D. K., Reddy N. A., Pettini
    M., 2005, ApJ, 626, 44
Swinbank A. M., Chapman S. C., Smail I., Lindner C., Borys C., Blain A. W.,
    Ivison R. J., Lewis G. F., 2006, MNRAS, 371, 465
Swinbank A. M., et al., 2008, MNRAS, 391, 420
Swinbank A. M., et al., 2010, MNRAS, 405, 234
Swinbank A. M., et al., 2014, MNRAS, 438, 1267
Tacconi L. J., et al., 2006, ApJ, 640, 228
Tacconi L. J., et al., 2010, Nature, 463, 781
Taniguchi Y., Shioya Y., 1998, ApJ, 501, L167
Toomre A., 1964, ApJ, 139, 1217
Trainor R. F., Steidel C. C., 2012, ApJ, 752, 39
```

#### APPENDIX A: FULL SPECTRAL MAP OF HS1700.850.1

Younger J. D., et al., 2008, ApJ, 688, 59

In this appendix, the full mosaic of CO emission line spectra are shown for each  $0.13^{\prime\prime}$  pixel in the HS1700.850.1 system. The line fitting code used to make the moment maps is described in Appendix B.

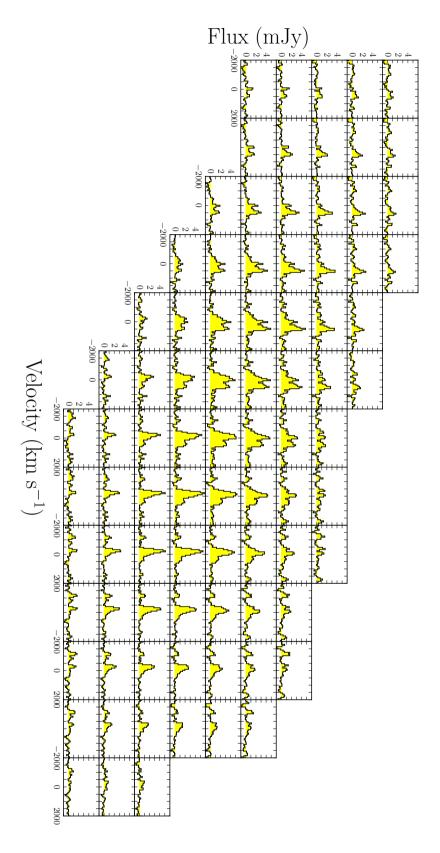


Figure A1. The full mosaic of 1D spectral extractions for the HS1700.850.1 system. Each box represents a pixel of 0.13'' (units of mJy per beam in each pixel), and the measurements extend over 1.7'' in RA and 1.3'' in DEC. The synthesized beam size is  $0.8'' \times 0.4''$  (§ 2.1) along a position angle 59 deg East of North.

# APPENDIX B: LINE FITTING / MOMENT MAP PYTHON CODE

Emission line fitting is a vital component for analyzing the kinematics of galaxies. By fitting Gaussian emission lines to the spectra, it allows us to determine the average velocity of the gas, integrated flux and the velocity dispersion of the galaxies at a specific location. Putting all these together, we can look at the total kinematics of the sources as a whole. The code used for the emission line fitting throughout the paper is compatible with python version 2.7. Below are the key points of the code and an explanation of how it works:

- The code initially extracts the data from the data cube, specifying the *x* and *y* pixel coordinates and the emission spectra for that specific pixel
- A radius is chosen for which the code looks to fit a Gaussian to the emission spectra, which it then loops over and discards any pixel with an integrated flux of  $< 3\sigma$
- The Gaussian profiles are fit using the scipy.optimize.curve\_fit function, which uses a nonlinear least squares fitting method to determine the best fit to the given data with a specified model.
- The first function to be fit to the spectra is a Gaussian plus continuum level, which is then subtracted off the total spectra
- The gaussian function is forced to try fitting at the maximum value of the spectra (i.e. the peak of the emission line and the average velocity of the gas) so it fits the correct portion of data. The dispersion is then determined by the fitting parameters calculated. The errors for each parameter are calculated through the scipy.optimize.curve\_fit function.
- Finally, the integrated velocity flux is calculated by integrating over the total emission line model once it has been fit
- Once this process has been completed for every pixel in the radius specified, moment maps are created by placing the values of each parameter in the corresponding pixel location of the galaxy

A sample code will be made available online.

This paper has been typeset from a TEX/IATEX file prepared by the author.